



CHORUS

This is the accepted manuscript made available via CHORUS. The article has been published as:

## Coupling Single Atoms to a Nanophotonic Whispering-Gallery-Mode Resonator via Optical Guiding

Xinchao Zhou, Hikaru Tamura, Tzu-Han Chang, and Chen-Lung Hung

Phys. Rev. Lett. **130**, 103601 — Published 7 March 2023

DOI: [10.1103/PhysRevLett.130.103601](https://doi.org/10.1103/PhysRevLett.130.103601)

# Coupling single atoms to a nanophotonic whispering-gallery-mode resonator via optical guiding

Xinchao Zhou,<sup>1</sup> Hikaru Tamura,<sup>1</sup> Tzu-Han Chang,<sup>1</sup> and Chen-Lung Hung<sup>1,2,\*</sup>

<sup>1</sup>*Department of Physics and Astronomy, Purdue University, West Lafayette, IN 47907, USA*

<sup>2</sup>*Purdue Quantum Science and Engineering Institute,  
Purdue University, West Lafayette, IN 47907, USA*

(Dated: February 7, 2023)

We demonstrate an efficient optical guiding technique for coupling cold atoms in the near field of a planar nanophotonic circuit, and realize large atom-photon coupling to a whispering-gallery mode in a microring resonator with a single-atom cooperativity  $C \gtrsim 8$ . The guiding potential is created by diffracted light on a nanophotonic waveguide that smoothly connects to a dipole trap in the far field for atom guiding with subwavelength precision. We observe atom-induced transparency for light coupled to a microring, characterize the atom-photon coupling rate, extract guided atom flux, and demonstrate on-chip photon routing by single atoms. Our demonstration promises new applications with cold atoms on a nanophotonic circuit for chiral quantum optics and quantum technologies.

Ultracold atoms strongly coupled to photonic fields are model systems for realizing quantum nonlinear optics [1], quantum networks [2, 3], and quantum simulations of many-body physics [4–6]. Interfacing cold atoms with nanoscale photonic waveguides [7–15] and resonators [16–27] in quasi-linear (1D) and planar (2D) geometries further promises stronger atom-light interactions and novel quantum functionalities via dispersion engineering, controlled photon propagation, topology, and chiral quantum transport, thus leading to new paradigms for quantum optics beyond conventional settings in cavity and waveguide quantum electrodynamics (QED) [28, 29].

To date, the key challenge for atom-nanophotonic integration remains to be efficient transporting and trapping of cold atoms on nanoscale dielectrics. Success so far has been limited to suspended 1D structures, which are surrounded by vacuum and allow for laser-cooled atoms to be loaded directly into optical traps in the near field (distance  $z \lesssim$  optical wavelength above surface). Examples include optical nanofibers [8, 9], where an array of atoms can be localized in a lattice of two-color evanescent field traps formed by guided light. Through external-illumination, a tight optical trap can also form on top of a suspended waveguide [15, 16, 23]. For deterministic atom trapping, optical tweezers or an optical conveyor belt have been utilized to initiate atom loading in freespace, followed by transport to a proximal photonic crystal [16, 30]. These guiding and trapping techniques enable demonstrations of cooperative atom-photon coupling [10–12, 15], and collective Lamb shifts with trapped atoms [31]. Waveguide-interfaced atomic quantum memories [13], photonic phase gate [18], and atom-photon/atom-atom entanglement [27] have also been realized.

Extending optical trapping to 2D photonic structures, however, faces immediate challenges. Due to restricted trap opening to freespace and reduced laser cooling ef-

iciency in the near field above a dielectric plane, potentially caused by unbalanced radiation pressure from surface reflection and scattering or from increased heating rates due to mechanical vibrations [32], unobstructed atom loading into a near field trap has shown limited success probability [33, 34]. This has prevented further explorations of atom-light coupling on more complex and interesting planar structures such as 2D photonic crystals [35] and whispering-gallery mode (WGM) microring resonators with propagation-direction-dependent, chiral atom-light interactions [36–38]. Without tackling the challenges of cooling and trapping, thermal atomic vapors have already been coupled to integrated ring resonators [39, 40] and waveguides [41–44], but with much limited single-atom interaction time and cooperativity.

In this letter, we overcome such restrictions using a technique for precision guiding of cold atoms from far field ( $z \gtrsim 250 \mu\text{m}$ ) to a nanoscale optical trap in the near field with subwavelength precision. This scheme is projected to work with generic dielectric nanostructures – a far-off resonant optical beam forms a tapered guiding potential towards a bottom-illuminated structure (Fig. 1), where diffracted light in the near field can precisely direct trapped atoms towards the surface like a geometrically defined ‘optical funnel’. We show that the end of an optical funnel ( $z \lesssim 100 \text{nm}$ ) can be plugged using a repulsive evanescent field potential that could also counteract atom-surface Casimir-Polder attraction to form a stable trap [Fig. 1(d)]. We implement an optical funnel for guiding cold atoms and coupling them, for the first time, to a nanophotonic microring resonator in a fiber-integrated circuit [45–47]. We achieve synchronous atom guiding towards a designated spot on a microring, and report observation of atom-photon coupling in a WGM of the microring resonator with single-atom cooperativity  $C \gtrsim 8$  during the atom-transit. We extract a peak atom flux  $\approx 240 \text{ms}^{-1}$ , under a peak atom-photon coupling rate  $g_{\text{max}}/(2\pi) \approx 136 \text{MHz}$  for a spin-polarized atom. Our scheme is complementary to an optical conveyor belt [30, 33], and can be extended to guiding and

---

\* clhung@purdue.edu

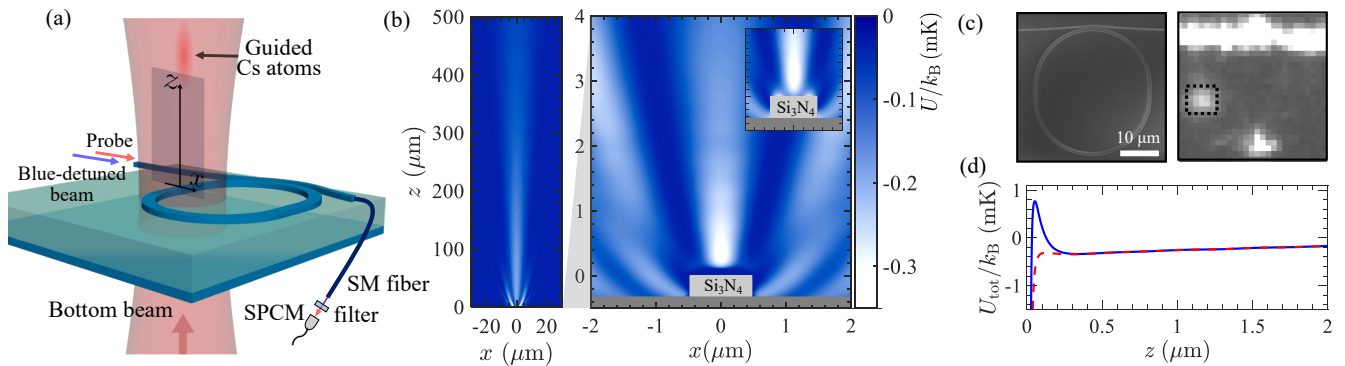


FIG. 1. Optical funnel on a nanophotonic microring circuit. (a) Schematic of the setup. An optical funnel is formed by a red-detuned, bottom-illuminating beam. WGMs in the microring are excited by a probe field co-propagating with a blue-detuned beam. The latter forms a repulsive potential barrier to plug the optical funnel. Transmitted light is directed to a single photon counting module (SPCM) after wavelength filtering. (b) Cross section of the funnel potential  $U(x, z)$  (left) and a zoom in view near the  $\text{Si}_3\text{N}_4$  waveguide (right). Inset shows the potential without a barrier (unplugged funnel). Gravity is along the  $-z$  direction. (c) Scanning electron micrograph of a microring (left), and an optical micrograph (right, same field of view) showing fluorescence from guided atoms (bounded by dashed box). Other bright spots are unfiltered scattered light from the waveguide. (d) Potential line cuts  $U_{\text{tot}}(0, z)$  with (solid curve) and without (dashed curve) the repulsive barrier.  $U_{\text{tot}} = U + U_{\text{cp}}$  includes the atom-surface Casimir-Polder potential  $U_{\text{cp}}$  [45].

trapping atom arrays in generic planar nanostructures.

We begin the experiment by collecting  $\sim 10^5$  laser-cooled cesium atoms (temperature  $\sim 20 \mu\text{K}$  following polarization gradient-cooling, PGC) at  $z \approx 250 \mu\text{m}$  above a transparent silica membrane that hosts a racetrack-shaped  $\text{Si}_3\text{N}_4$  microring resonator [45, 48]. The atoms are loaded into an optical funnel that points towards the microring waveguide of width  $\approx 950 \text{ nm}$  and height  $\approx 326 \text{ nm}$ , respectively. The funnel potential is formed in a red-detuned, bottom-illuminating beam (wavelength  $\lambda_r \approx 935.3 \text{ nm}$ ), with a beam waist of  $7 \mu\text{m}$  and a polarization locally parallel to the waveguide. Over the top, the zeroth-order diffraction exhibits strong intensity gradient, diffracting from a  $200 \text{ nm}$   $1/e^2$ -transverse width into a circular far-field dipole beam profile; see Fig. 1(b) and [45]. This guiding potential in the near field is robust against beam misalignment by more than the width of the microring waveguide ( $\gtrsim 1 \mu\text{m}$ ), which we confirmed in simulation and experimentally. Higher order diffractions do not form funnels because they display intensity maxima that are several micrometers away from the waveguide. Localized atoms in the optical funnel can be fluorescence imaged at distances  $z \lesssim 10 \mu\text{m}$  [33, 34], as shown in Fig. 1(c).

We plug the optical funnel using a repulsive evanescent field formed by a ‘blue’ WGM (wavelength  $\lambda_b \approx 849.55 \text{ nm}$ ). A plugged funnel potential exhibits a stable trap minimum in the near field. We adjust the power of the bottom beam,  $P_r \approx 15 \text{ mW}$ , and that of the blue-detuned beam,  $P_b \approx 33 \mu\text{W}$ , to form a closed trap with trap minimum at  $z \approx 280 \text{ nm}$  and a trap depth of  $k_B \times 250 \mu\text{K}$ , where  $k_B$  is the Boltzmann constant; see Fig. 1(d).

We detect guided atoms in the near field by probing atom-WGM photon interactions. The ‘probe’ WGM res-

onance is thermally stabilized to the  $F = 4 \leftrightarrow F' = 5$  transition in D2 line. Probe photons are sent through one end of a bus waveguide to couple to the clockwise circulating (CW) WGM (coupling rate  $\kappa_e \approx 2\pi \times 0.77 \text{ GHz}$ ). The intrinsic photon loss rate is  $\kappa_i \approx 2\pi \times 0.95 \text{ GHz}$ , and the total photon loss rate is  $\kappa = \kappa_e + \kappa_i \approx 2\pi \times 1.72 \text{ GHz}$  [45]. Resonant probe photons are drawn into the microring and dissipate, reducing the bus waveguide transmission to  $T_0 = |(\kappa_e - \kappa_i)/\kappa|^2 \approx 0.01$ . Interaction with an atom will lead to an increased transparency  $T > T_0$  [45, 49]. We note that a WGM photon is nearly circular-polarized in the near field. Interaction with the probe WGM (in CW circulation) can thus drive  $\sigma^+$  transitions with spin axis defined transversely to the waveguide; an atom can also emit a photon in the counter-clockwise circulating (CCW) WGM via the  $\sigma^-$  transitions, inducing reflection in the bus waveguide; see discussions in [45]. In our microring, CW and CCW WGM resonances are degenerate.

Our probe sequence is illustrated in Fig. 2 inset. We prepare atoms in the  $F = 4$  ground state and then shut off the PGC light, allowing them to be guided towards the microring surface. After a wait time  $\Delta t$ , two weak probe pulses are sent through the bus waveguide, each with a duration of  $1 \text{ ms}$ , to measure the transmission  $T$  ( $T_0$ ) in the presence (absence) of atoms; the bottom beam is switched off for  $3 \text{ ms}$  between the two pulses to release guided atoms. Each experiment is repeated 100 times for averaging.

In Fig. 2, we observe increased transmission and a clear maximum up to  $T \approx 0.26$  at  $\Delta t \approx 5 \text{ ms}$ , indicating a peak atom flux arriving at the near field. Interestingly, transmission resurges at  $16 \text{ ms} \lesssim \Delta t \lesssim 21 \text{ ms}$ . This is due to longitudinal reflection of most guided atoms in a rapidly narrowing optical funnel [50, 51], regardless of

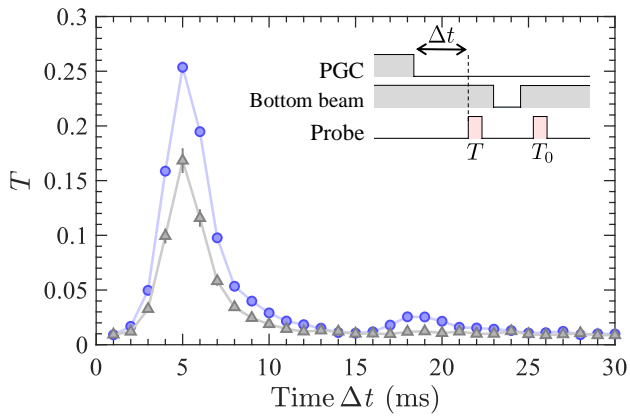


FIG. 2. Atom guiding in the optical funnel. Resonant transmission  $T$  versus guiding time  $\Delta t$  in a plugged (circles) and unplugged (triangles) funnel, respectively. Experimental sequence is illustrated in the inset.

the presence of the repulsive potential barrier. These reflected atoms are later drawn back towards the surface for recoupling. We have performed atomic trajectory simulations [52] to confirm the observed oscillatory behavior and guiding effect [45].

We note that transparency is more pronounced with coupling to guided atoms in a plugged optical funnel, due to the fact that a repulsive barrier can increase the atom-WGM photon interaction time. To see this, in Fig. 3(a) we overlay sample atomic trajectories and position-dependent atom-photon coupling strength  $\bar{g}$ , calculated using the CW WGM field distribution [53] and averaged over  $g$  of all magnetic sub-levels [45]. Note that  $\bar{g}$  is constant along the waveguide ( $y$ -axis). Most trajectories exhibit a longitudinal classical turning point in the near field  $z = 110 \pm 20$  nm and within  $|x| \lesssim 0.3$   $\mu\text{m}$ . Corresponding time-dependent coupling strengths  $\bar{g}(t)$  are plotted in Fig. 3(b). Averaging over all trajectories, we find peak  $\bar{g}_{\text{max}} \approx 2\pi \times 97$  MHz, corresponding to a peak cooperativity  $\bar{C}^+ = 4\bar{g}_{\text{max}}^2/\kappa/\gamma \approx 4.2$ . Here  $\gamma = 2\pi \times 5.2$  MHz is the atomic decay rate in freespace. The averaged interaction time (root-mean-square time weighted by interaction strength) would approach  $t_i^b \approx 2$   $\mu\text{s}$ , more than doubled from  $t_i \approx 0.9$   $\mu\text{s}$  for typical trajectories without a repulsive barrier.

To further experimentally characterize guided atoms in the near field, we vary the probe detuning  $\Delta\nu$  and measure the transmission spectra at  $\Delta t = 5$  ms [Fig. 3(c)]. With the repulsive barrier, it appears that the transmission spectrum is slightly asymmetric and is red-shifted by  $\approx 5$  MHz from freespace resonance ( $\Delta\nu = 0$ ). This is attributed to the position-dependent light shift induced by the blue-detuned beam; the closer the atom is to the surface, the larger the red-shift. We note that there is negligible light shift from the guiding beam, because  $\lambda_r$  is near the magic wavelength for D2 transition [9]. We measure a peak transmission  $T \approx 0.26$  and a broad linewidth  $\approx 30$  MHz  $> \gamma/2\pi$ . This can be com-

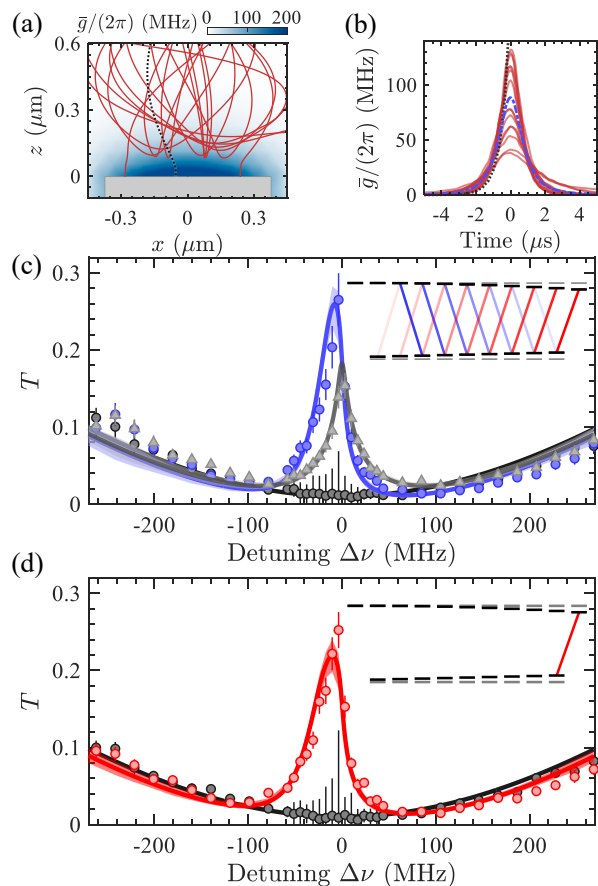


FIG. 3. Atom-WGM photon interaction. (a) Sample trajectories (solid curves) in the near field. False color map shows unpolarized atom-photon coupling strength  $\bar{g}$ . (b)  $\bar{g}$  versus time for sample trajectories; blue dash-dotted curve is the mean. Black dotted curves in (a-b) show a typical case without the repulsive barrier. The time origin is aligned with the time to have the largest coupling strength for each trajectory. (c) Measured transmission  $T$  versus laser detuning  $\Delta\nu$  for unpolarized atoms with (blue circles) and without (gray triangles) the repulsive barrier, and  $T_0$  for bare resonator without atoms. Solid blue (gray) curve is a single parameter fit using Eq. (1) and input from trajectory calculations as in (a-b) with (without) the repulsive barrier. Shaded band shows 95% pointwise confidence level. (d) Measured and fitted transmission  $T$  versus laser detuning  $\Delta\nu$  for polarized atoms in a plugged funnel. Insets in (c-d) illustrate the levels involved in the  $F = 4 \leftrightarrow F' = 5$  transition.

pared to the case without a repulsive barrier, which gives a symmetric lineshape with smaller peak  $T \approx 0.15$  but an even broader linewidth  $\approx 37$  MHz. We can attribute the reduced transparency in the unplugged funnel to the shorter interaction time  $t_i^b < t_i$  per atom transit. However, the larger linewidth could result from an increased cooperativity and a larger Purcell broadening  $\approx (1 + \bar{C})\gamma$ , where  $\bar{C} = \bar{C}^+ + \bar{C}^-$  is the total cooperativity for coupling to both CW-WGM and CCW-WGM.  $\bar{C}^- \approx 0.5\bar{C}^+$  for an unpolarized level scheme in Fig. 3(c) [45].

The observed transparency is induced by a continu-

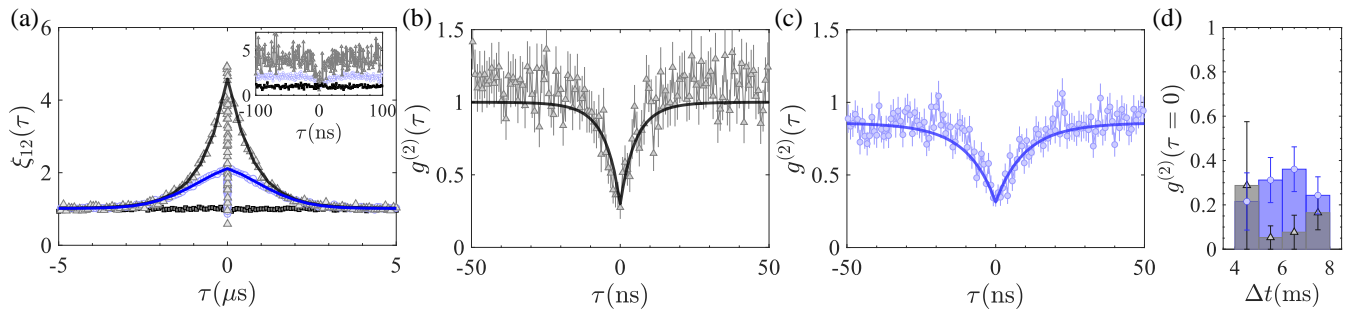


FIG. 4. Correlation measurement for the resonant transmission. (a) Cross-correlation  $\xi_{12}(\tau)$  of two detector counts in the Hanbury-Brown-Twiss setup. Gray triangles (blue circles) show the data obtained with guided atoms in the unplugged (plugged) optical funnel, while black squares show the background  $\xi_{12} \approx 1$  obtained without guided atoms. Black and blue lines are bidirectional exponential fits to the data. Inset provides a zoom-in view in the range of  $|\tau| \leq 100$  ns. During the detection of atom-transits, normalized intensity correlation functions  $g^{(2)}(\tau)$  show clear anti-bunching for (b) unplugged and (c) plugged optical funnels, respectively. Solid lines are theoretical fits [45], giving effectively time-averaged single-atom cooperativities  $C^+ \approx 8$  and 3 for atom-transits in (b) and (c), respectively. Black (blue) bars in (d) show the measured  $g^{(2)}(0)$  as a function of guiding time  $\Delta t$  in the unplugged (plugged) optical funnel.

ous stream of atoms interacting with the microring. To extract the guided atom flux in the optical funnel, we fit the measured spectra by calculating a time-averaged transmission signal

$$\frac{T}{T_0} = 1 + \mathcal{N} \left[ \frac{\langle \int \mathcal{T}(\Delta\nu, g(t)) dt \rangle}{\int \mathcal{T}(\Delta\nu, 0) dt} - 1 \right], \quad (1)$$

where  $\mathcal{T}(\Delta\nu, g)$  is the steady-state transmission [45],  $\langle \dots \rangle$  denotes averaging over trajectories calculations as shown in Fig. 3(a-b), and we have taken into account time- and state-dependent atom-photon coupling as well as light shifts. This model fits well to the measured line shape, using the flux  $\mathcal{N}$  as the only adjustable parameter. In either case in Fig. 3(c), we find  $\mathcal{N} \approx 600 \text{ ms}^{-1}$ , giving near unity  $\mathcal{N}t_i^{(b)} \approx 0.5 - 1.2$ . This suggests we have nearly continuous single-atom transits during the entire 1 ms probe window.

We have also measured transmission spectrum using spin-polarized atoms in the  $|F=4, m_F=4\rangle$  ground state [Fig. 3(d)], which would have the largest coupling to the CW WGM due to the  $\sigma^+$  cycling transition. The spectrum indeed shows a broader linewidth ( $\approx 40$  MHz), in accordance with a larger peak cooperativity  $C = C^+ \approx 8.2$  with peak  $g_{\text{max}}/(2\pi) \approx 136$  MHz for the  $\sigma^+$  transition. Here the fitted atom flux is reduced to  $\mathcal{N} \approx 240 \text{ ms}^{-1}$ , likely due to the loss of guided atoms during the optical pumping process.

To see if the transmitted photons are indeed routed by single atoms one at a time, we perform Hanbury-Brown-Twiss correlation measurements [54] on resonant transmissions with polarized atoms. In order to do this, the transmitted photon stream is directed from the bus waveguide to an optical fiber with  $\gtrsim 80\%$  efficiency [46] and then detected by two single-photon counters following a 50/50 beam splitter. We calculate the intensity

cross-correlation by

$$\xi_{12}(\tau) = \left\langle \frac{I_1(\Delta t)I_2(\Delta t + \tau)}{I_1(\Delta t) \cdot I_2(\Delta t + \tau)} \right\rangle, \quad (2)$$

where  $I_{1,2}(t)$  is the time-stamped photon counts from each detector using a 0.8 ns time bin,  $\bar{\phantom{x}}$  and  $\langle \dots \rangle$  denote averaging over time  $\Delta t$  (within a 2 ms window) and repeated experiments, respectively. The measured  $\xi_{12}(\tau)$  shows a peak in the microsecond-timescale with guided atoms in Fig. 4(a), indicating positive classical correlations in transmitted photons during atom-transits through the evanescence region of the WGM. Using a bidirectional exponential fit, we extract the full width to be 2.4  $\mu\text{s}$  (1.0  $\mu\text{s}$ ) with (without) the repulsive barrier, which is in good agreement with the simulated atom-transit time in Fig. 3(b). The larger peak correlation measured with the unplugged funnel qualitatively reflects the larger photon scattering rate  $\sim C^+\gamma$  during the atom transit. Most importantly, there is a sharp reduction of photon correlations near the central 20 ns window, suggesting the presence of one photon affects the transport of another near the time scale of atom-photon interactions – similar to a photon-blockade effect [54, 55]. Nonetheless,  $\xi_{12}(0)$  does not dip below the shot-noise level,  $\xi_{12}(0) = 1$ , because the residual classical photon correlation is due to the stochastic nature of randomly arriving single atoms and the finite  $\sim 1\%$  transmission of the uncoupled microring resonator.

To confirm single atom-photon coupling, we extract possible non-classical photon correlations during each detection of atom-transit. We first identify atom-transit events in the time-stamped signals by imposing a threshold of 2 counts within a 1.6  $\mu\text{s}$  running window. We then analyze the normalized intensity correlation  $g^{(2)}(\tau)$ , similar to Eq. (2), but using signals in a 2  $\mu\text{s}$  window centered around each post-selected transit events. For details, see the Supplemental Material [45]. In Fig. 4(b-

c), we indeed observe significant photon anti-bunching  $g^{(2)}(0) = 0.27(8)$  and  $0.35(5)$ , respectively, without and with the repulsive barrier. Photon anti-bunching in the resonant transmission signal can be regarded as a signature of single atom coupling to the WGM photons [54]. The observed stronger anti-bunching signal in an unplugged funnel again results from a larger time-averaged cooperativity  $C^+ \approx 8$ , which we determined from a theory fit [45]. We also confirm that photon anti-bunching can be observed over an extended time period whenever there are guided atoms coupled to the microring [Fig. 4(d)];  $g^2(0)$  remains nearly at a constant level, including the time around  $\Delta t \approx 5$  ms when we observe the peak atom flux. This suggests the transmitted photons observed in Figs. 2-3 are indeed routed by single atoms, one at a time, instead of multiple atoms simultaneously coupled to the same resonator mode, in which we expect more complex behavior in photon correlations. Nonetheless, correlated photon transport gated by multiple atoms is an interesting topic in its own right [56, 57]. This can be studied using multiple optical funnels formed on a microring resonator.

In conclusion, we have demonstrated an optical trapping technique that guides single atoms on a planar nanophotonic resonator with subwavelength precision. Using our technique, single atom trapping probabil-

ity may be improved by pulsing on a lattice beam [15, 16, 23, 26, 33] to localize atoms in the near field following an instantaneous feedback from probing a WGM resonator [26]. To further cool and localize single atoms in a near field trap, evanescent-wave cooling [58, 59], Raman sideband cooling [60, 61], or cavity cooling [62, 63] may be implemented. The achieved single-atom, single-mode (CW-WGM) cooperativity  $C^+ \gtrsim 8$  is currently limited by the quality factor  $Q \approx 2 \times 10^5$  of the coupled microring circuit. We expect significant improvement in the cooperativity parameter by more than 5-fold with a better  $Q > 10^6$  [34, 48] following improvements in waveguide surface roughness and material quality. Our work would enable new applications, for example, in chiral quantum optics [21, 22, 36, 64–67] based on cold atoms coupled to an on-chip WGM resonator. Our system also holds a promise for realizing photon-mediated atom-atom interactions and quantum many-body physics [5, 6, 68–71] with multiple trapped atoms.

We thank B. M. Fields and M. E. Kim for their prior contribution to the experiment. This work was supported by the AFOSR (Grant NO. FA9550-17-1-0298, FA9550-22-1-0031), the ONR (Grant NO. N00014-17-1-2289), and a seed fund from Purdue Quantum Science and Engineering Institute. H.T. and C.-L.H. acknowledge support from the NSF (Grant NO. PHY-1848316).

- 
- [1] D. E. Chang, V. Vuletić, and M. D. Lukin, Quantum nonlinear optics – photon by photon, *Nature Photonics* **8**, 685 (2014).
  - [2] H. J. Kimble, The quantum internet, *Nature* **453**, 1023 (2008).
  - [3] A. Reiserer and G. Rempe, Cavity-based quantum networks with single atoms and optical photons, *Rev. Mod. Phys.* **87**, 1379 (2015).
  - [4] H. Ritsch, P. Domokos, F. Brennecke, and T. Esslinger, Cold atoms in cavity-generated dynamical optical potentials, *Rev. Mod. Phys.* **85**, 553 (2013).
  - [5] J. S. Douglas, H. Habibian, C.-L. Hung, A. V. Gorshkov, H. J. Kimble, and D. E. Chang, Quantum many-body models with cold atoms coupled to photonic crystals, *Nature Photonics* **9**, 326 (2015).
  - [6] A. González-Tudela, C.-L. Hung, D. E. Chang, J. I. Cirac, and H. J. Kimble, Subwavelength vacuum lattices and atom–atom interactions in two-dimensional photonic crystals, *Nature Photonics* **9**, 320 (2015).
  - [7] M. Kohnen, M. Succo, P. G. Petrov, R. A. Nyman, M. Trupke, and E. A. Hinds, An array of integrated atom–photon junctions, *Nature Photonics* **5**, 35 (2011).
  - [8] E. Vetsch, D. Reitz, G. Sagué, R. Schmidt, S. T. Dawkins, and A. Rauschenbeutel, Optical interface created by laser-cooled atoms trapped in the evanescent field surrounding an optical nanofiber, *Phys. Rev. Lett.* **104**, 203603 (2010).
  - [9] A. Goban, K. S. Choi, D. J. Alton, D. Ding, C. Lacroûte, M. Pototschnig, T. Thiele, N. P. Stern, and H. J. Kimble, Demonstration of a state-insensitive, compensated nanofiber trap, *Phys. Rev. Lett.* **109**, 033603 (2012).
  - [10] H. L. Sørensen, J.-B. Béguin, K. W. Kluge, I. Iakoupov, A. S. Sørensen, J. H. Müller, E. S. Polzik, and J. Appel, Coherent backscattering of light off one-dimensional atomic strings, *Phys. Rev. Lett.* **117**, 133604 (2016).
  - [11] N. V. Corzo, B. Gouraud, A. Chandra, A. Goban, A. S. Sheremet, D. V. Kupriyanov, and J. Laurat, Large Bragg reflection from one-dimensional chains of trapped atoms near a nanoscale waveguide, *Phys. Rev. Lett.* **117**, 133603 (2016).
  - [12] P. Solano, P. Barberis-Blostein, F. K. Fatemi, L. A. Orozco, and S. L. Rolston, Super-radiance reveals infinite-range dipole interactions through a nanofiber, *Nature Communications* **8**, 1857 (2017).
  - [13] N. V. Corzo, J. Raskop, A. Chandra, A. S. Sheremet, B. Gouraud, and J. Laurat, Waveguide-coupled single collective excitation of atomic arrays, *Nature* **566**, 359 (2019).
  - [14] A. Goban, C.-L. Hung, S.-P. Yu, J. D. Hood, J. A. Muniz, J. H. Lee, M. J. Martin, A. C. McClung, K. S. Choi, D. E. Chang, O. Painter, and H. J. Kimble, Atom–light interactions in photonic crystals, *Nature Communications* **5**, 3808 (2014).
  - [15] A. Goban, C.-L. Hung, J. D. Hood, S.-P. Yu, J. A. Muniz, O. Painter, and H. J. Kimble, Superradiance for atoms trapped along a photonic crystal waveguide, *Phys. Rev. Lett.* **115**, 063601 (2015).
  - [16] J. D. Thompson, T. G. Tiecke, N. P. de Leon, J. Feist, A. V. Akimov, M. Gullans, A. S. Zibrov, V. Vuletić, and M. D. Lukin, Coupling a single trapped atom to a nanoscale optical cavity, *Science* **340**, 1202 (2013).
  - [17] C. Junge, D. O’Shea, J. Volz, and A. Rauschenbeutel,

- Strong coupling between single atoms and nontransversal photons, *Phys. Rev. Lett.* **110**, 213604 (2013).
- [18] T. G. Tiecke, J. D. Thompson, N. P. de Leon, L. R. Liu, V. Vuletić, and M. D. Lukin, Nanophotonic quantum phase switch with a single atom, *Nature* **508**, 241 (2014).
- [19] J. Volz, M. Scheucher, C. Junge, and A. Rauschenbeutel, Nonlinear  $\pi$  phase shift for single fibre-guided photons interacting with a single resonator-enhanced atom, *Nature Photonics* **8**, 965 (2014).
- [20] S. Kato and T. Aoki, Strong coupling between a trapped single atom and an all-fiber cavity, *Phys. Rev. Lett.* **115**, 093603 (2015).
- [21] M. Scheucher, A. Hilico, E. Will, J. Volz, and A. Rauschenbeutel, Quantum optical circulator controlled by a single chirally coupled atom, *Science* **354**, 1577 (2016).
- [22] O. Bechler, A. Borne, S. Rosenblum, G. Guendelman, O. E. Mor, M. Netser, T. Ohana, Z. Aqua, N. Drucker, R. Finkelstein, Y. Lovsky, R. Bruch, D. Gurovich, E. Shafir, and B. Dayan, A passive photon-atom qubit swap operation, *Nature Physics* **14**, 996 (2018).
- [23] K. P. Nayak, J. Wang, and J. Keloth, Real-time observation of single atoms trapped and interfaced to a nanofiber cavity, *Phys. Rev. Lett.* **123**, 213602 (2019).
- [24] D. H. White, S. Kato, N. Német, S. Parkins, and T. Aoki, Cavity dark mode of distant coupled atom-cavity systems, *Phys. Rev. Lett.* **122**, 253603 (2019).
- [25] P. Samutpraphoot, T. Đorđević, P. L. Ocola, H. Bernien, C. Senko, V. Vuletić, and M. D. Lukin, Strong coupling of two individually controlled atoms via a nanophotonic cavity, *Phys. Rev. Lett.* **124**, 063602 (2020).
- [26] E. Will, L. Masters, A. Rauschenbeutel, M. Scheucher, and J. Volz, Coupling a single trapped atom to a whispering-gallery-mode microresonator, *Phys. Rev. Lett.* **126**, 233602 (2021).
- [27] T. Đorđević, P. Samutpraphoot, P. L. Ocola, H. Bernien, B. Grinkemeyer, I. Dimitrova, V. Vuletić, and M. D. Lukin, Entanglement transport and a nanophotonic interface for atoms in optical tweezers, *Science* **373**, 1511 (2021).
- [28] D. E. Chang, J. S. Douglas, A. González-Tudela, C.-L. Hung, and H. J. Kimble, Colloquium: Quantum matter built from nanoscopic lattices of atoms and photons, *Rev. Mod. Phys.* **90**, 031002 (2018).
- [29] A. S. Sheremet, M. I. Petrov, I. V. Iorsh, A. V. Poshakinskiy, and A. N. Poddubny, Waveguide quantum electrodynamics: collective radiance and photon-photon correlations (2021), arXiv:2103.06824 [quant-ph].
- [30] A. P. Burgers, L. S. Peng, J. A. Muniz, A. C. McClung, M. J. Martin, and H. J. Kimble, Clocked atom delivery to a photonic crystal waveguide, *Proceedings of the National Academy of Sciences* **116**, 456 (2019).
- [31] J. D. Hood, A. Goban, A. Asenjo-Garcia, M. Lu, S.-P. Yu, D. E. Chang, and H. J. Kimble, Atom-atom interactions around the band edge of a photonic crystal waveguide, *Proceedings of the National Academy of Sciences* **113**, 10507 (2016).
- [32] D. Hümmer, P. Schneeweiss, A. Rauschenbeutel, and O. Romero-Isart, Heating in nanophotonic traps for cold atoms, *Phys. Rev. X* **9**, 041034 (2019).
- [33] M. E. Kim, T.-H. Chang, B. M. Fields, C.-A. Chen, and C.-L. Hung, Trapping single atoms on a nanophotonic circuit with configurable tweezer lattices, *Nature Communications* **10**, 1647 (2019).
- [34] H. Tamura, T.-H. Chang, X. Zhou, B. Fields, M. Zhu, and C.-L. Hung, Microring resonators on a suspended membrane circuit for atom-light interactions, in *Integrated Optics: Devices, Materials, and Technologies XXV*, Vol. 11689, International Society for Optics and Photonics (SPIE, 2021) pp. 174 – 179.
- [35] S.-P. Yu, J. A. Muniz, C.-L. Hung, and H. J. Kimble, Two-dimensional photonic crystals for engineering atom-light interactions, *Proceedings of the National Academy of Sciences* **116**, 12743 (2019).
- [36] P. Lodahl, S. Mahmoodian, S. Stobbe, A. Rauschenbeutel, P. Schneeweiss, J. Volz, H. Pichler, and P. Zoller, Chiral quantum optics, *Nature* **541**, 473 (2017).
- [37] C. Junge, D. O’shea, J. Volz, and A. Rauschenbeutel, Strong coupling between single atoms and nontransversal photons, *Physical review letters* **110**, 213604 (2013).
- [38] I. Shomroni, S. Rosenblum, Y. Lovsky, O. Bechler, G. Guendelman, and B. Dayan, All-optical routing of single photons by a one-atom switch controlled by a single photon, *Science* **345**, 903 (2014).
- [39] L. Stern, R. Zektzer, N. Mazurski, and U. Levy, Enhanced light-vapor interactions and all optical switching in a chip scale micro-ring resonator coupled with atomic vapor, *Laser & Photonics Reviews* **10**, 1016 (2016).
- [40] R. Ritter, N. Gruhler, W. H. P. Pernice, H. Kübler, T. Pfau, and R. Löw, Coupling thermal atomic vapor to an integrated ring resonator, *New Journal of Physics* **18**, 103031 (2016).
- [41] W. Yang, D. B. Conkey, B. Wu, D. Yin, A. R. Hawkins, and H. Schmidt, Atomic spectroscopy on a chip, *Nature Photonics* **1**, 331 (2007).
- [42] L. Stern, B. Desiatov, N. Mazurski, and U. Levy, Strong coupling and high-contrast all-optical modulation in atomic cladding waveguides, *Nature Communications* **8**, 14461 (2017).
- [43] R. Ritter, N. Gruhler, H. Dobbertin, H. Kübler, S. Scheel, W. Pernice, T. Pfau, and R. Löw, Coupling thermal atomic vapor to slot waveguides, *Phys. Rev. X* **8**, 021032 (2018).
- [44] A. Skljarow, H. Kübler, C. S. Adams, T. Pfau, R. Löw, and H. Alaian, Purcell-enhanced dipolar interactions in nanostructures, *Phys. Rev. Res.* **4**, 023073 (2022).
- [45] See Supplemental Material at ... for discussions on detailed experimental setup, characterization of the microring circuit, data analysis procedures, and theoretical models, which includes Refs. [72–78].
- [46] T.-H. Chang, X. Zhou, H. Tamura, and C.-L. Hung, Realization of efficient 3D tapered waveguide-to-fiber couplers on a nanophotonic circuit, *Opt. Express* **30**, 31643 (2022).
- [47] T.-H. Chang, X. Zhou, M. Zhu, B. M. Fields, and C.-L. Hung, Efficiently coupled microring circuit for on-chip cavity QED with trapped atoms, *Applied Physics Letters* **117**, 174001 (2020).
- [48] T.-H. Chang, B. M. Fields, M. E. Kim, and C.-L. Hung, Microring resonators on a suspended membrane circuit for atom-light interactions, *Optica* **6**, 1203 (2019).
- [49] T. Aoki, B. Dayan, E. Wilcut, W. P. Bowen, A. S. Parkins, T. J. Kippenberg, K. J. Vahala, and H. J. Kimble, Observation of strong coupling between one atom and a monolithic microresonator, *Nature* **443**, 671 (2006).
- [50] B. K. Teo and G. Raithel, Atom reflection in a tapered magnetic guide, *Phys. Rev. A* **65**, 051401 (2002).

- [51] J. Poulin, P. S. Light, R. Kashyap, and A. N. Luiten, Optimized coupling of cold atoms into a fiber using a blue-detuned hollow-beam funnel, *Phys. Rev. A* **84**, 053812 (2011).
- [52] We perform trajectory simulations in the  $x$ - $z$  plane. Motion along the  $y$ -axis is less relevant due to symmetry of the waveguide, the large dipole beam waist  $7\ \mu\text{m}$ , and its long Rayleigh length  $z_R \approx 165\ \mu\text{m}$ .
- [53] Multiphysics software for optimizing designs.
- [54] B. Dayan, A. S. Parkins, T. Aoki, E. P. Ostby, K. J. Vahala, and H. J. Kimble, A photon turnstile dynamically regulated by one atom, *Science* **319**, 1062 (2008).
- [55] K. M. Birnbaum, A. Boca, R. Miller, A. D. Boozer, T. E. Northup, and H. J. Kimble, Photon blockade in an optical cavity with one trapped atom, *Nature* **436**, 87 (2005).
- [56] A. Sipahigil, R. E. Evans, D. D. Sukachev, M. J. Burek, J. Borregaard, M. K. Bhaskar, C. T. Nguyen, J. L. Pacheco, H. A. Atikian, C. Meuwly, R. M. Camacho, F. Jelezko, E. Bielejec, H. Park, M. Lončar, and M. D. Lukin, An integrated diamond nanophotonics platform for quantum-optical networks, *Science* **354**, 847 (2016).
- [57] D. M. Lukin, M. A. Guidry, J. Yang, M. Ghezellou, S. D. Mishra, H. Abe, T. Ohshima, J. Ul-Hassan, and J. Vučković, Optical superradiance of a pair of color centers in an integrated silicon-carbide-on-insulator microresonator (2022).
- [58] P. Desbiolles, M. Arndt, P. Szriftgiser, and J. Dalibard, Elementary Sisyphus process close to a dielectric surface, *Phys. Rev. A* **54**, 4292 (1996).
- [59] Y. B. Ovchinnikov, I. Manek, and R. Grimm, Surface trap for Cs atoms based on evanescent-wave cooling, *Phys. Rev. Lett.* **79**, 2225 (1997).
- [60] Y. Meng, A. Dureau, P. Schneeweiss, and A. Rauschenbeutel, Near-ground-state cooling of atoms optically trapped 300 nm away from a hot surface, *Phys. Rev. X* **8**, 031054 (2018).
- [61] V. Vuletić, C. Chin, A. J. Kerman, and S. Chu, Degenerate Raman sideband cooling of trapped cesium atoms at very high atomic densities, *Phys. Rev. Lett.* **81**, 5768 (1998).
- [62] P. Maunz, T. Puppe, I. Schuster, N. Syassen, P. W. H. Pinkse, and G. Rempe, Cavity cooling of a single atom, *Nature* **428**, 50 (2004).
- [63] M. Hosseini, Y. Duan, K. M. Beck, Y.-T. Chen, and V. Vuletić, Cavity cooling of many atoms, *Phys. Rev. Lett.* **118**, 183601 (2017).
- [64] I. Shomroni, S. Rosenblum, Y. Lovsky, O. Bechler, G. Guendelman, and B. Dayan, All-optical routing of single photons by a one-atom switch controlled by a single photon, *Science* **345**, 903 (2014).
- [65] S. Mahmoodian, P. Lodahl, and A. S. Sørensen, Quantum networks with chiral-light-matter interaction in waveguides, *Phys. Rev. Lett.* **117**, 240501 (2016).
- [66] C. Gonzalez-Ballester, A. Gonzalez-Tudela, F. J. Garcia-Vidal, and E. Moreno, Chiral route to spontaneous entanglement generation, *Phys. Rev. B* **92**, 155304 (2015).
- [67] H. Pichler, T. Ramos, A. J. Daley, and P. Zoller, Quantum optics of chiral spin networks, *Phys. Rev. A* **91**, 042116 (2015).
- [68] S. Gopalakrishnan, B. L. Lev, and P. M. Goldbart, Frustration and glassiness in spin models with cavity-mediated interactions, *Phys. Rev. Lett.* **107**, 277201 (2011).
- [69] C.-L. Hung, A. González-Tudela, J. I. Cirac, and H. J. Kimble, Quantum spin dynamics with pairwise-tunable, long-range interactions, *Proceedings of the National Academy of Sciences* **113**, E4946 (2016).
- [70] E. J. Davis, G. Bentsen, L. Homeier, T. Li, and M. H. Schleier-Smith, Photon-mediated spin-exchange dynamics of spin-1 atoms, *Phys. Rev. Lett.* **122**, 010405 (2019).
- [71] Y. Guo, R. M. Kroeze, V. D. Vaidya, J. Keeling, and B. L. Lev, Sign-changing photon-mediated atom interactions in multimode cavity quantum electrodynamics, *Phys. Rev. Lett.* **122**, 193601 (2019).
- [72] E. R. Abraham and E. A. Cornell, Teflon feedthrough for coupling optical fibers into ultrahigh vacuum systems, *Applied optics* **37**, 1762 (1998).
- [73] F. Le Kien, P. Schneeweiss, and A. Rauschenbeutel, Dynamical polarizability of atoms in arbitrary light fields: general theory and application to cesium, *The European Physical Journal D* **67**, 92 (2013).
- [74] D. A. Steck, Cesium D line data (2003).
- [75] J.-T. Shen and S. Fan, Theory of single-photon transport in a single-mode waveguide. i. coupling to a cavity containing a two-level atom, *Phys. Rev. A* **79**, 023837 (2009).
- [76] J.-T. Shen and S. Fan, Theory of single-photon transport in a single-mode waveguide. ii. coupling to a whispering-gallery resonator containing a two-level atom, *Phys. Rev. A* **79**, 023838 (2009).
- [77] T. Li, A. Miranowicz, X. Hu, K. Xia, and F. Nori, Quantum memory and gates using a  $\Lambda$ -type quantum emitter coupled to a chiral waveguide, *Phys. Rev. A* **97**, 062318 (2018).
- [78] H. J. Carmichael, *Statistical methods in quantum optics 2: Non-classical fields* (Springer Science & Business Media, 2009).